Book of Tutorials and Abstracts

European Microbeam Analysis Society

EMAS 2019

16th

EUROPEAN WORKSHOP

on

MODERN DEVELOPMENTS AND APPLICATIONS IN MICROBEAM ANALYSIS

19 to 23 May 2019
at the
NTNU, Realfagbygget
Trondheim, Norway

Organised in collaboration with:
Norwegian University of Science and Technology
(NTNU)

A DICTIONARY INDEXING APPROACH FOR EBSD

Mark De Graef

Carnegie Mellon University, Department of Materials Science and Engineering
130 Roberts Engineering Hall, 5000 Forbes Avenue, 15213-3890 Pittsburgh, PA, U.S.A.
e-mail: mdg@andrew.cmu.edu

Marc De Graef received his BSc-and MSc-degrees in physics from the University of Antwerp (Belgium) in 1983, and his PhD in physics from the Catholic University of Leuven (Belgium) in 1989. After three and a half years as a post-doctoral researcher in the Materials Department at the University of California at Santa Barbara, he joined Carnegie Mellon University in 1993, where he currently is a full professor and co-director of the J. Earle and Mary Roberts Materials Characterization Laboratory Facility. His research interests lie in the area of microstructural characterisation of structural intermetallics and magnetic materials. His current focus is on the development of experimental and modelling techniques for the quantitative study of magnetic domain configurations and a theoretical analysis of the use of shape functions in the computation of shape-dependent material properties. A second research focus is on the acquisition and representation of the three-dimensional character of microstructures. Work in this area includes development of accurate forward models for many different characterisation modalities. He has published more than 300 papers as well as two textbooks. He is a Fellow of the Microscopy Society of America.

1. ABSTRACT

Dictionary indexing is a new approach to the indexing of electron backscatter diffraction (EBSD) patterns. In this contribution, we will describe the underlying forward model as well as the indexing approach that uses a similarity metric between experimental and simulated patterns instead of feature extraction. Then we provide a number of example applications drawn from the materials and geological communities.

2. INTRODUCTION

Historically, electron backscatter diffraction patterns were indexed manually before commercial indexing packages based on the Hough transform became available in the early 1990s. Today, Hough-based indexing can be carried out rapidly (several thousand patterns per second), and produces accurate orientations, provided the detector geometry has been characterised accurately and the patterns have a sufficiently high signal-to-noise ratio. In 2015, we proposed a new indexing approach [1] that does not extract any features from the experimental patterns; instead, the approach matches complete simulated patterns, using a physics-based forward modelling approach, against the experimental patterns, and assigns the crystal orientation of the best matching pattern, using one of many image similarity metrics, to the experimental pattern. In this contribution, we will briefly review the components of the forward model as well as the basic dictionary indexing (DI) algorithm and we will illustrate the approach with a number of concrete examples drawn from both the materials and geological communities. We will illustrate the robustness of the DI approach against pattern noise as well as the ability of the technique to distinguish between materials with nearly identical crystal structure. We will conclude with a short preview of a recently developed, more efficient indexing approach that is based on the forward model combined with spherical harmonic Fourier transforms.

3. SUMMARY OF THE EBSD FORWARD MODEL

Simulated EBSD patterns can be obtained using a physics-based forward model [2-4] consisting of: (1) a Monte Carlo simulation of the spatial, energy, and depth distributions of the backscattered electrons (BSEs); (2) a dynamical (quantum-mechanical) simulation of the channelling of the BSEs on their way out of the sample; and (3) an accurate geometrical model for the sample-detector configuration. Without going into details, the model produces the BSE yield on a spherical surface (the Kikuchi sphere) surrounding an imaginary spherical single crystal with an electron source with a range of energies at its centre; this intensity distribution represents the EBSD Master Pattern (MP) and is shown in Fig. 1a for Ni at 20 kV. Individual EBSD patterns are then determined by direct interpolation for a given crystal orientation and detector geometry. The spherical nature of the data immediately suggests the use of spherical harmonic functions to generate an indexing scheme; we will briefly describe such an approach

at the end of this contribution. To simplify interpolations from the master pattern, we convert the spherical intensity data via a 2D equal-area Lambert projection [5] onto a square (Fig. 1b), which allows for direct bilinear instead of spherical interpolation. Typical pattern generation rates range from a few hundred to several thousand patterns per second, depending on the individual pattern size and the number of compute threads used.

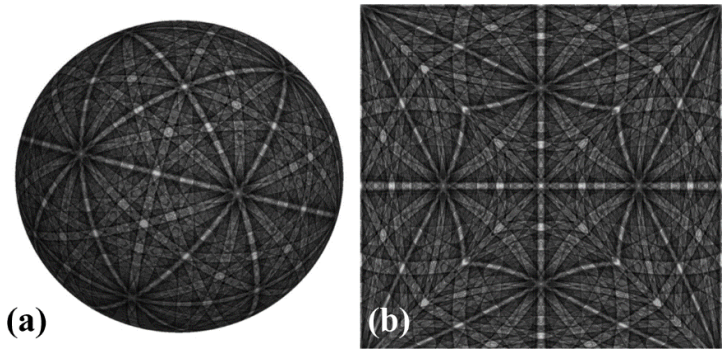

Figure 1. a) Kikuchi sphere for nickel at 20 kV; b) square Lambert projection for the Northern hemisphere of a).

4. THE PRINCIPLES BEHIND DICTIONARY INDEXING

Dictionary Indexing (DI) refers to an algorithm to compare complete experimental EBSD patterns against simulated patterns, using one of many potential image similarity metrics. This approach requires two initial steps, namely the generation of a uniform sample of orientations, and a basic pattern pre-processing step. We will describe both steps in the following subsections, followed by a demonstration of the robustness of this indexing technique against noise. Then we describe the approach as a dimensionality reduction scheme and we introduce a number of useful derived maps. We conclude the section with a brief description of orientation refinement as a post-processing step.

4.1. Orientation space sampling

The EBSD forward model is used in combination with a uniform sampling approach for orientation space *SO(3)* [7] to generate a collection of EBSD patterns for a given angular sampling step size. The sampling algorithm operates in the cubochoric orientation representation, an equal-volume mapping of the quaternion Northern hemisphere onto a cubic grid. Since uniform samples on a cubic grid are trivial to generate, using the cubochoric approach naturally leads to an efficient sampling algorithm. For each point on the grid, the orientation is transformed to a Rodrigues-Frank vector, and this vector is then tested against the geometry of the fundamental zone (FZ) for the particular crystal symmetry under consideration; if the point lies outside the FZ it is discarded from the list, otherwise it remains on the list. Once the list is complete, an individual EBSD pattern is computed for each orientation; the collection of these patterns is referred to as the "pattern dictionary". The number of patterns in a dictionary can

become quite large, in particular for low-symmetry crystal structures; for an orientation sampling step size of 1.4°, there are 333,227 unique patterns for cubic crystal symmetry, and 8,000,000 patterns for triclinic symmetry. This is likely the most important drawback of the DI approach and is partially remedied by the new spherical harmonic approach described at the end of this contribution.

4.2. Pattern pre-processing

Before the DI algorithm is applied, both experimental and dictionary patterns undergo two pre-processing steps. The first step is a standard high-pass Fourier filter that eliminates most of the background contrast variations in the patterns. The second step increases the contrast in the patterns by applying an adaptive histogram equalisation (AHE) filter [8] that changes the usually Gaussian-like intensity histogram to an essentially uniform histogram, so that all intensity levels between 0 and 255 are approximately equally present in the pattern. This step increases the differences between pairs of patterns, making it more likely that the indexing process will recover the correct result. Both pre-processing steps are carried out on all experimental and dictionary patterns before the patterns are compared to each other.

4.3. Robustness against noise

Each of the dictionary patterns is then compared to each of the experimental patterns using either a normalised dot product or the mutual information [9] between the two patterns. Since each pattern is represented by a unit vector, simply taking the dot product between two pattern vectors produces a measure for the similarity of the two patterns, in the same way that the dot product between two unit 3D vectors is a measure for the angle between the two vectors (a smaller angle or larger dot product indicates an increased similarity between the vectors). The orientation of the dictionary pattern for which the similarity metric is highest is taken to be the orientation of the illuminated volume. Repeating this process for all experimental patterns then indexes the entire data set [1].

Figure 2 shows an example of the robustness of the dictionary indexing approach for a Ni data set (courtesy of S. Wright) recorded using four different detector settings, with the signal-to-noise ratio decreasing from top left to bottom right. Even for the noisiest patterns, for which the Hough approach largely fails, the full pattern dot product similarity metric provides a viable means of indexing the patterns, with an 85 % indexing success rate. This rate can be brought close to 100 % by performing a non-local means filter to the data before applying the DI algorithm [10]. Hence, the dictionary approach overcomes limitations that are inherent to the traditional Hough-based indexing algorithm; this robustness indicates that patterns from heavily deformed materials are now no longer impossible to index.

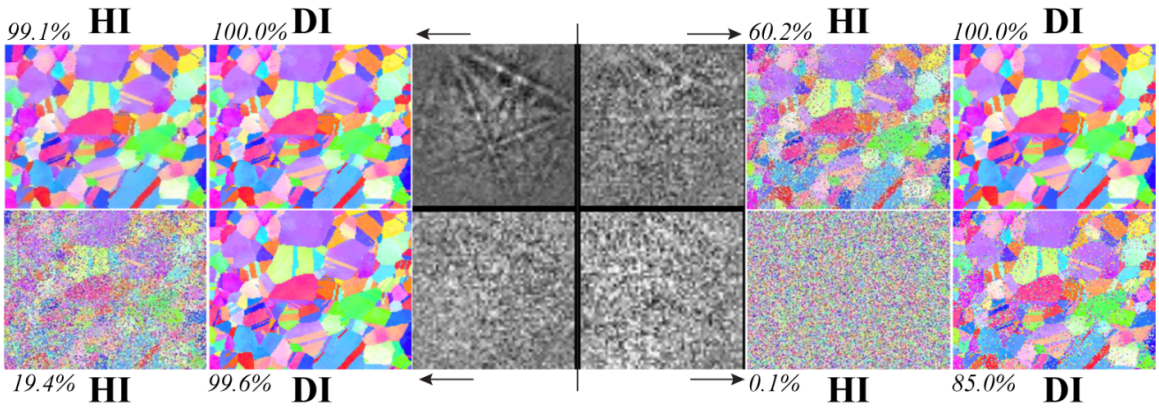

Figure 2. Indexing examples using Hough indexing (HI) and Dictionary Indexing (DI) for four different pattern qualities; the percentages indicate the indexing success-rate of each approach. (Data courtesy S. Wright).

3.4. DI as a dimensionality reduction algorithm

An EBSD pattern of M by N pixels with intensities in the range [0 … 255] can be regarded formally as a point in a discrete MN-dimensional space. Indexing the EBSD pattern essentially means that we need to reduce the dimensionality of the pattern from *MN* to 3, since there are three parameters needed to uniquely describe a 3D orientation. This is a significant reduction in dimensionality, even for the smallest patterns typically acquired using 8x binning; if the binned pattern size is 80 by 60 pixels, then the necessary reduction is from 4,800 to 3. This indicates that there should be more than sufficient information in an EBSD pattern, even after 8x or higher binning, to make it possible to index the pattern. Indeed, in our analysis of the performance of the DI approach under a number of different conditions we found that even binning down to patterns of size 15 by 15 pixels does not substantially degrade the indexing success rate or the angular accuracy [11]. Considering EBSD indexing to be a form of dimensionality reduction suggests that the technique may benefit from modern machine learning (ML) approaches, in particular convolutional neural nets (CNNs); the EBSD forward model can be used to generate as many patterns as are needed to properly train the CNN. In our preliminary work, we have shown that reasonable indexing success rates can be achieved by means of machine learning techniques [12]; the main drawback of ML, however, is the lengthy training cycle that is required to set up the neural net (several days of GPU time for a given set of detector parameters and crystal structure). This suggests that machine-learning approaches may have only limited applicability for real-time EBSD indexing.

3.5. Derived maps

The DI approach can be used to generate a number of maps that are not readily available using the Hough-based technique. After the pattern pre-processing step, one can compute the Average

Dot Product (ADP) map, i.e., a map that shows the average dot product of each pattern vector with its four nearest neighbours (for square grid sampling). The intensity in the ADP map is given by:

$$\alpha_{r,c} = \frac{1}{4}(\hat{\boldsymbol{v}}_{r,c}.\hat{\boldsymbol{v}}_{r+1,c} + \hat{\boldsymbol{v}}_{r,c}.\hat{\boldsymbol{v}}_{r-1,c} + \hat{\boldsymbol{v}}_{r,c}.\hat{\boldsymbol{v}}_{r,c+1} + \hat{\boldsymbol{v}}_{r,c}.\hat{\boldsymbol{v}}_{r,c-1}),$$

where each unit vector represents a pattern and the subscripts indicate the pattern position in the inverse pole figure map. The ADP map (example shown in Fig. 3a for a portion of a 20 kV forsterite data set, courtesy of K. Marquardt) is quite sensitive to the similarity between neighbouring patterns and highlights both microstructural features (e.g., grain boundaries, different phases) and sample artefacts (e.g., surface scratches) [13].

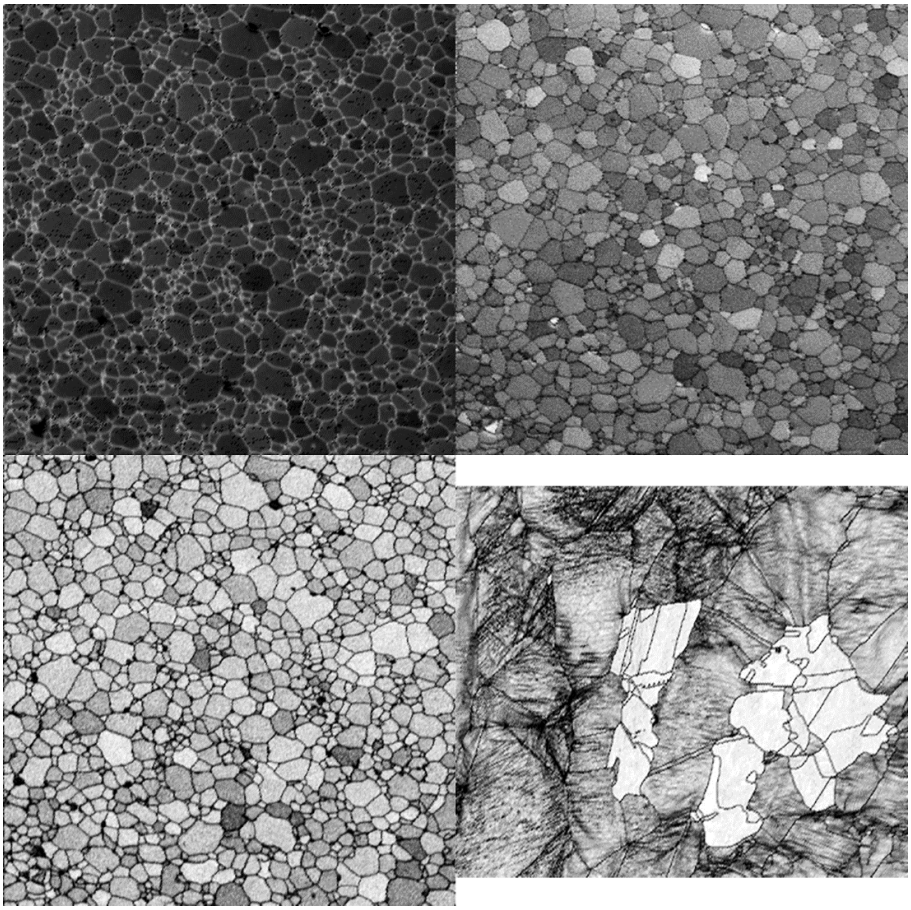

Figure 3. Forsterite maps: a) inverted ADP map, b) CI map, and c) OSM map. d) OSM map for partially recrystallised CuZn.

During indexing, one maintains, for each experimental pattern, a list of the dictionary patterns that are similar to it, ranked by decreasing similarity metric. The best matching pattern produces

the most likely orientation, and the corresponding similarity metric value can be used to generate a Confidence Index (CI) map (example for forsterite shown in Fig. 3b). The list of N next nearest matches can be used to generate an Orientation Similarity Map (OSM), i.e., a map that shows how similar the top matches list of a given pattern is to those of its nearest neighbours. If $S_{r,c}$ is a set containing the list of N top-matching dictionary pattern labels for the pattern at sampling location (r,c), then the OSM value is defined using the following relation (again for a square sampling grid):

$$\eta_{r,c} = \frac{1}{4}\left(\#(S_{r,c} \cap S_{r-1,c}) + \#(S_{r,c} \cap S_{r+1,c}) + \#(S_{r,c} \cap S_{r,c-1}) + \#(S_{r,c} \cap S_{r,c+1})\right).$$

In this equation, # represents the cardinality of the intersection set between the top lists for two neighbouring sampling points. The OSM map provides a remarkably clear microstructure map outlining sharply defined grain boundaries, as is shown in Fig. 3c for the forsterite data set. Figure 3d shows the OSM for a deformed and partially recrystallised Cu-Zn sample (10 kV, data set courtesy M. Taheri); note that the recrystallised grains clearly stand out against the background of deformed grains. The contrast between the two sets of grains is readily explained: for a recrystallised grain, neighbouring points have nearly identical top-matching sets $S_{r,c}$, whereas for heavily deformed grains, the list of top matches varies strongly from point to point, thus generating a significantly lower orientation similarity value.

3.6. Orientation refinements

The standard DI algorithm produces the best match on a cubochoric sampling grid of orientations for which the dictionary patterns were computed. The true orientation for a given experimental pattern is likely to lie between sampling grid points, so the final step in the indexing process is a refinement of the orientation. This is carried out using a quadratic bounded optimisation algorithm [14] and results in orientation accuracies on the order of 0.1°. During refinement, one can also carry out the pattern centre correction, since the dictionary patterns are computed using only one single pattern centre for all patterns. This correction is not very important when the sampled region of interest has a size that is similar to the detector pixel size, but for a larger field of view, the correction becomes quite important, as has been shown in [14].

3.7. Background and related information

The DI technique and its foundation and applications have been described in detail in a series of publications which we list here as reference for the interested reader: generation of a reliable orientation space sampling scheme that is uniform in the equal-volume sense [15]; detailed analysis of the accuracy and precision of the DI technique, in particular with respect to pattern size and other detector parameters [14]; introduction of an orientation refinement scheme that allows for accurate indexing of large-area EBSD data sets [14]; introduction of a robust phase differentiation scheme based on the DI approach [16]; extension of the DI approach to electron channeling patterns (ECP) [15]; and the first application of DI to transmission Kikuchi

diffraction (TKD) patterns [17]; successful application of the DI technique to distinguish between dynamically and post-dynamically recrystallized grains in an Inconel 718 sample, showing an orientation angular resolution, after refinement, of about 0.1° [18]; indexing of a three-phase geological sample, consisting of garnet (cubic), clinopyroxene (monoclinic), and an amorphous glassy phase wetting some of the grain boundaries [13].

4. EXAMPLE APPLICATIONS ON METALLIC AND GEOLOGICAL MATERIALS

4.1. Grain boundaries in shot-peened aluminium

Figure 4 shows a [001] inverse pole figure map for Hough and dictionary indexing (HI and DI) of a portion of a 10 kV shot-peened Al 7075 data set (courtesy T. Burnett), about 30 µm away from the sample surface; the acquisition step size was 23 nm. Red pixels in (a) indicate un-indexed points (using the Aztec software); they belong to two groups: points near the grain boundaries and points clustered at second phase precipitates. In the dictionary indexing result, all points have been indexed (except for points inside the precipitates) and the grain boundaries are more clearly delineated, as is shown in the magnified views of the region around a triple junction. Occasional points near the boundaries are mis-indexed as belonging to a neighbouring grain; such points can easily be corrected by standard clean-up procedures. This result indicates that the DI approach can handle overlap EBSD patterns without significant issues. The sharpness of the boundaries in the DI result can be improved by performing a statistical analysis on the top *N* matches, and selecting the orientation that is present the most in this set.

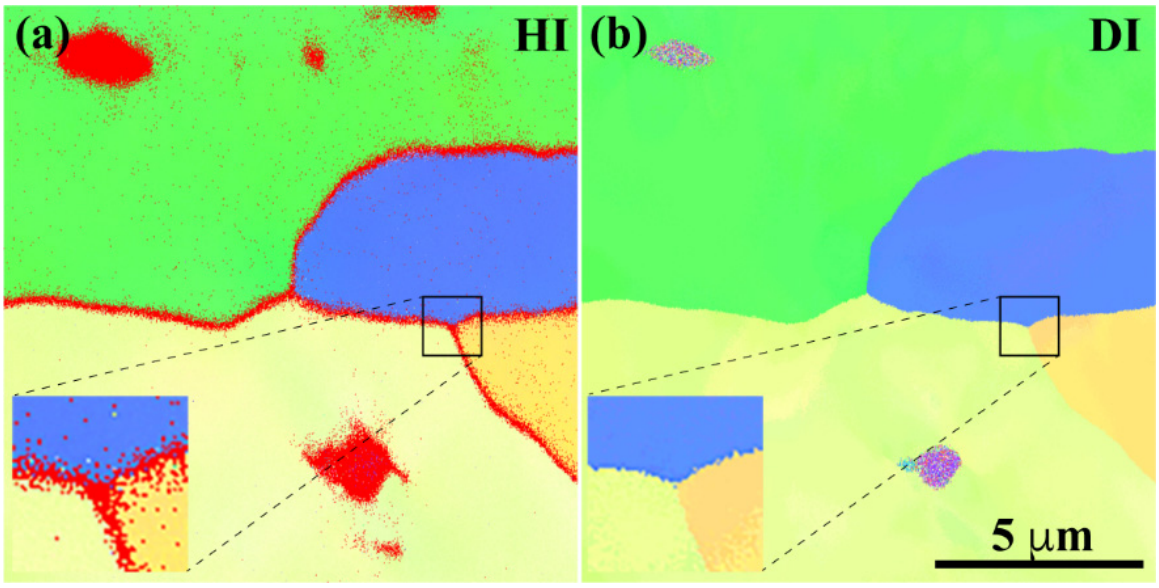

Figure 4. Grain boundaries in a [001] inverse pole figure for a shot-peened Al 7075, indexed using the Hough-based technique (HI) and the dictionary approach (DI). The insets show results near a triple junction.

4.2. Distinguishing between face-centred cubic phases

Face-centred cubic (fcc) materials produce nearly identical EBSD patterns for a given crystal orientation. A comparison of master patterns for Ag and Ni reveals that there are sufficient differences in intensity along the Kikuchi bands for the DI approach to be able to differentiate between the phases. Figure 5 shows the results of DI analysis of a 7 kV data set for de-wetted Ag on a polycrystalline Ni substrate (sample courtesy D. Chatain; unpublished research); (a) is the ADP map, (b) and (d) shows the Ni and Ag OSM maps that are combined into the phase map in (c) (Ni is red, Ag green). An example experimental 7 kV EBSD pattern is shown in (f) along with the simulated pattern in (e). An analysis of the confidence index values (top dot products) reveals that the differences between the two phases are well above the variation of the top dot product within each individual phase.

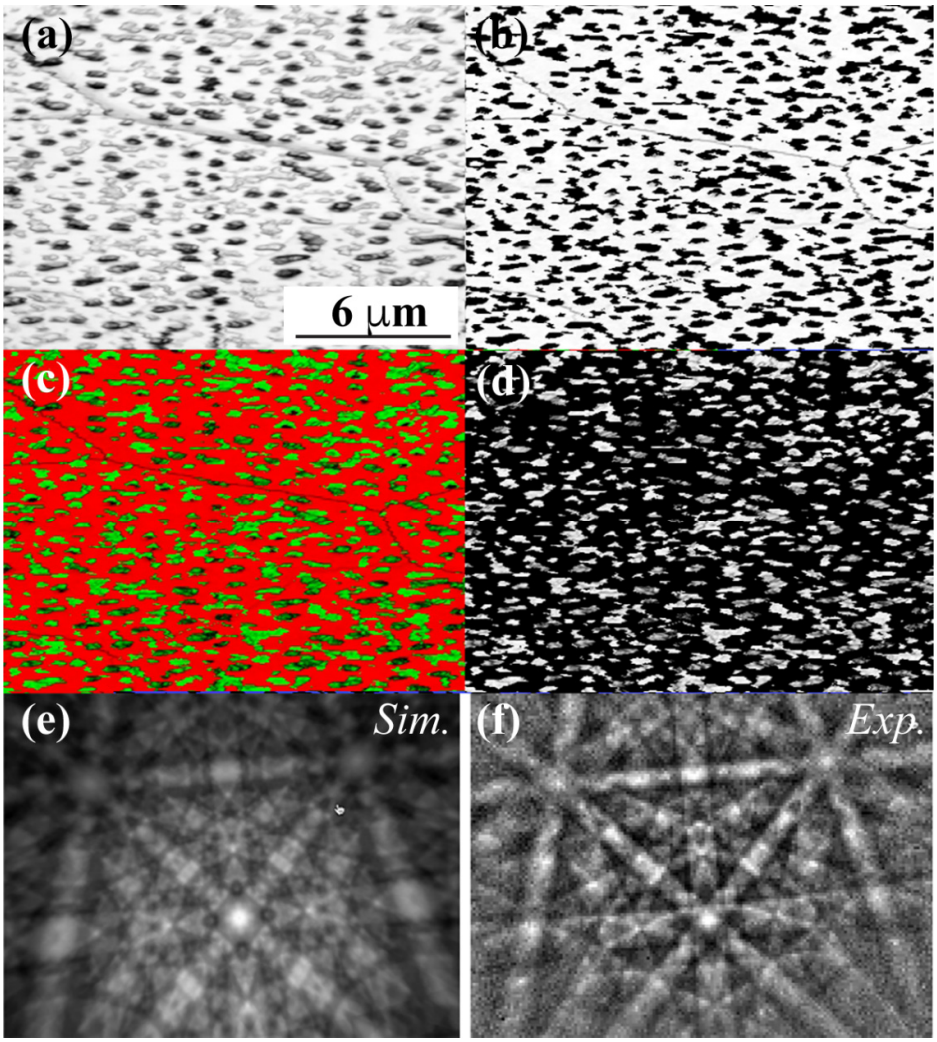

Figure 5. DI results for de-wetted Ag on polycrystalline Ni, 7 kV, 40 nm step size; a) ADP map; b and d) Ni and Ag OSM maps; c) phase map (Ni red, Ag, green); e and f) are simulated and experimental EBSD patters for Ag.

4.3. A multi-phase geological sample

The final example concerns a multi-phase geological sample consisting of garnet (grt, cubic), clinopyroxene (cpx, monoclinic) and an amorphous melt phase [13]. Since the melt phase does not produce patterns with Kikuchi bands, it is relatively easy to distinguish it from the other two phases simply from the ADP map shown in Fig. 6a.

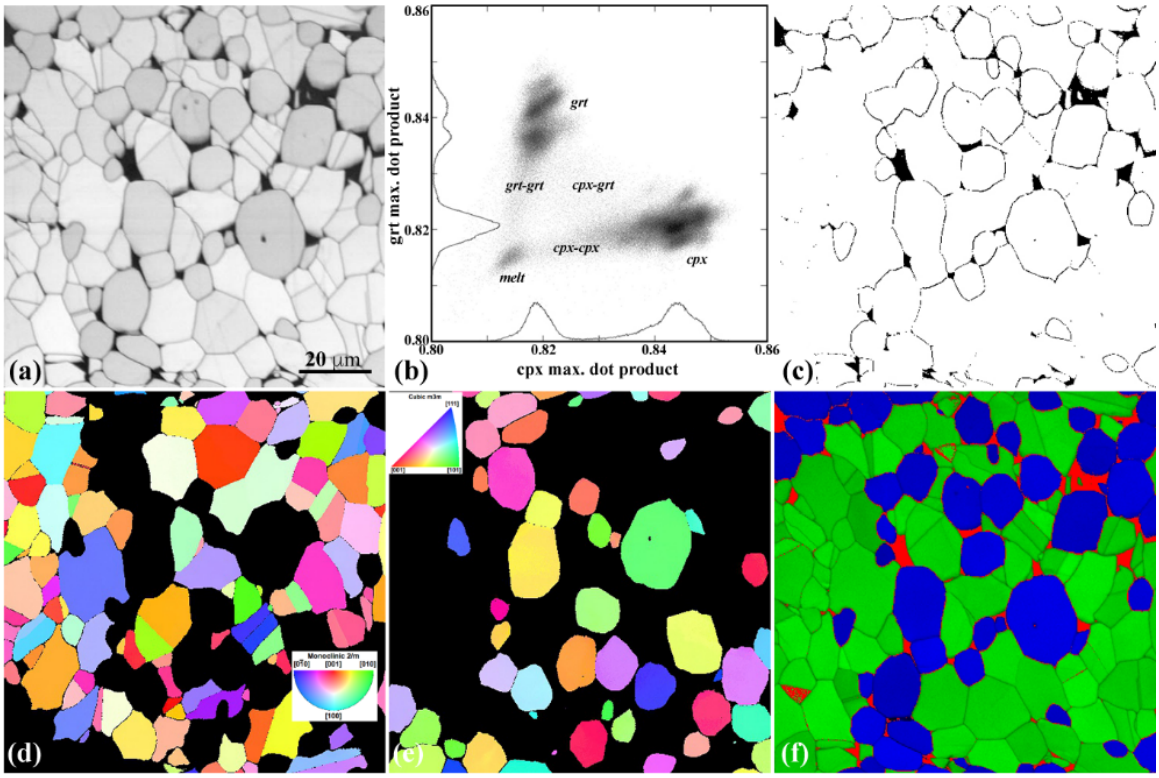

Figure 6. a) ADP map; b) maximum dot product histogram; c) melt phase; d and e) [001] IPF maps for cpx and grt; f) phase map (cpx = green, grt = blue, melt = red).

Application of the DI algorithm using master patterns for each of the phases (cpx and grt) results in two separate best-fit dot product values for each phase; Fig. 6b shows a 2D histogram of all dot product pairs. Several point clusters are clearly identified: patterns that match neither cpx nor grt likely correspond to the melt phase, whereas large clusters are present for each of the two phases. Each large cluster consists of smaller lumps of points, and detailed analysis shows that each lump corresponds to an individual grain. The diffuse area between the large clusters corresponds to grain boundary pixels, and there are three different types: cpx-cpx, grt-grt, and cpx-grt boundaries. Figure 6c shows the locations of the melt, derived from the histogram in (b). The bottom row of Fig. 6 shows the [001] IPF maps for cpx (d) and grt (e) (with colour legends as insets), as well as the combined phase map (f); note that the cpx-grt grain boundaries are wetted by the melt, whereas cpx-cpx or grt-grt boundaries are not wetted.

Figure 7a shows a portion of the OSM map for the cpx-grt-melt sample; the line between A and B crosses a cpx-cpx grain boundary. In Fig. 7b, a total of 40 points is sampled between A and B, and the number of near matches (out of a maximum of 20) that each indexing result has in common with each of the end members A and B is displayed; obviously, the end points have all 20 nearest matches in common with themselves. Moving closer to the grain boundary, the number of matches in common with the end point drops slightly until the grain boundary is reached, at which point the number drops to zero. The intersection of the two profiles can be used to determine the location of the grain boundary with an accuracy of better than a single sampling pixel.

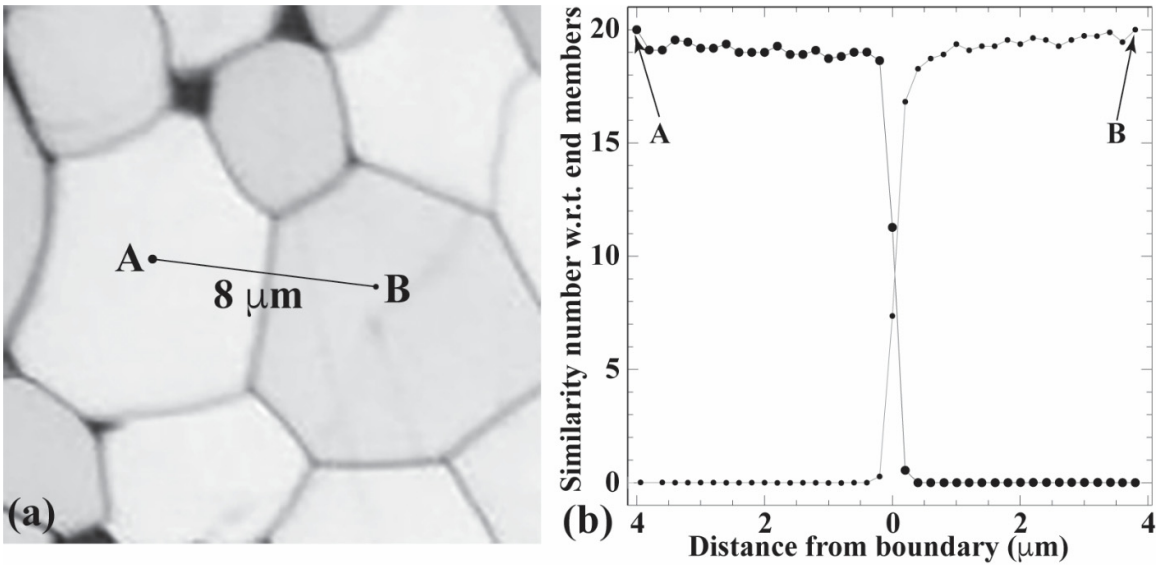

Figure 7. a) Portion of the cpx-grt ADP map with a trace across a cpx-cpx grain boundary between the points A and B; b) number of nearest matches that each sampling point has in common with each of the end members.

5. *A BRIEF LOOK AT THE FUTURE*

As the dictionary indexing approach becomes more widely used, we anticipate that the algorithm will be optimised for speed by using multiple GPUs combined with smarter pre-processing of the patterns; in the current scheme, each experimental pattern is considered to be fully independent of all other patterns, so that the incorporation of simple clustering schemes could already have a significant impact on the indexing speed. Since much of EBSD research deals with deformed materials, the next step in the development of the DI approach is the incorporation of deformation into the pattern interpolation scheme, so that a refinement of the pattern match with respect to the full deformation tensor becomes a possibility; this work is currently ongoing.

As noted in section 2, the EBSD forward model needs to be further developed to make the result more realistic, in particular with regards to the spectroscopic properties of the patterns. Ideally, this would involve solving the Yoshioka equations for elastic/inelastic electron scattering in combination with appropriate depth and energy integration schemes. This is a challenging problem, but progress in this area would also have a significant impact outside the EBSD field.

We have recently developed an alternative for the DI approach based on the fact that the master pattern resides on the Kikuchi sphere. Simply back projecting each experimental pattern onto the sphere and then carrying out a spherical correlation analysis using a spherical harmonic decomposition of the master pattern results in an efficient indexing algorithm that no longer requires the computation of any dictionary patterns and is thus nearly independent of the symmetry of the crystal structure. We anticipate that this spherical indexing approach, which we call "EMSphInx", may be capable of near real-time indexing at speeds comparable to the currently used Hough transform algorithm, but with the same increased robustness against noise displayed by the dictionary indexing approach. We are currently exploring the strengths and weaknesses of this new algorithm.

6. CONCLUDING REMARKS

The dictionary indexing and related algorithms are available in open source form as part of the author's EMsoft project; all source code (a combination of fortran-95, OpenMP, and OpenCL, with C/C++ wrapper routines) can be downloaded from a GitHub repository (https://github.com/EMsoft-org), and an extensive collection of EMsoft-related links, including example applications, is maintained at https://vbff.materials.cmu.edu/EMsoft. Test executable packages ("betas") are made available each night for Mac OS X and Windows 10 platforms from the following URL: http://www.bluequartz.net/binaries/EMsoft/experimental. The DI approach is currently being integrated into one of the EBSD vendor packages and will be available to the community for extensive testing and applications. Much progress is being made in quantitative EBSD research as well as in related SEM-based diffraction techniques; it is truly an exciting time to be working in the EBSD field!

7. ACKNOWLEDGMENTS

The author would like to acknowledge numerous colleagues who have over the years contributed ideas or data sets to the EBSD dictionary indexing project, among others S. Singh, F. Ram, W. Lenthe, E. Pascal, P. Callahan, M. Echlin, T. Pollock, M. Jackson, A. Hero, J. Simmons, S. Wright, K. Marquardt, M. Taheri, D. Chatain, P. Wynblatt, and T. Burnett. The author would like to acknowledge financial support from a DoD Vannevar-Bush Faculty Fellowship (#N00014-16-1-2821) as well as the computational facilities of the Materials Characterization Facility at CMU under grant #MCF-677785.

8. REFERENCES

[1] Chen Y H, *et al.* 2015 A dictionary approach to EBSD indexing. *Microsc. Microanal.* **21** 739-752

[2] Winkelmann A 2009 Principles of depth-resolved Kikuchi pattern simulation for electron backscatter diffraction. *J. Microsc.* 239 32-45

[3] Maurice C, *et al.* 2011 A method for accurate localisation of EBSD pattern centres. *Ultramicroscopy* **111** 140-148

[4] Callahan P G and De Graef M 2013 Dynamical EBSD patterns. Part I: Pattern simulations. *Microsc. Microanal.* **19** 1255-1265

[5] Roşca D 2010 New uniform grids on the sphere. *Astronomy Astrophys.* **520** A63-A63

[6] Singh S, *et al.* 2017 EMsoft: Open source software for electron diffraction/image simulations. *Microsc. Microanal.* **23** (Suppl. 1) 212-213

[7] Singh S and De Graef M 2016 Orientation sampling for dictionary-based diffraction pattern indexing methods. *Modeling Simulations Mater. Sci. Engng.* **24** 085013

[8] Pizer S M, *et al.* 1987 Adaptive histogram equalization and its variation. *Computer Vision, Graph. Image Process.* **39** 355-368

[9] Gulsoy E B, *et al.* 2009 Application of joint histogram and mutual information to registration and data fusion problems in serial sectioning microstructure studies. *Scripta Materialia* **60** 381-384

[10] Brewick P T W, Wright S I and Rowenhorst D J 2019 NLPAR: Non-local smoothing for enhanced EBSD pattern indexing. *Ultramicroscopy* **200** 50-61

[11] Ram F, *et al.* 2017 Error analysis of crystal orientations obtained by the dictionary approach to EBSD indexing. *Ultramicroscopy* **181** 17-26

[12] Jha D, *et al.* 2018 Extracting grain orientations from EBSD patterns of polycrystalline materials using convolutional neural networks. *Microsc. Microanal.* **24** 497-502

[13] Marquardt K, *et al.* 2017 Quantitative electron backscatter diffraction (EBSD) data analyses using the dictionary indexing (DI) approach: overcoming indexing difficulties in gological materials. *Amer. Mineralogist* **102** 1843-1855

[14] Singh S, *et al.* 2017 Application of forward models to crystal orientation refinement. *J. Appl. Crystall.* **50** 1664-1676

[15] Singh S and De Graef M 2017 Dictionary indexing of electron channeling patterns. *Microsc. Microanal.* **23** 1-12

[16] Ram F and De Graef M 2018 Phase differentiation by electron backscatter diffraction using the dictionary indexing approach. *Acta Materialia* **144** 352-364

[17] Pascal E, *et al.* 2018 Energy-weighted dynamical scattering simulations of back-scattered electron diffraction modalities. *Ultramicroscopy* **187** 98-106

[18] Nicolaÿ A, *et al.* 2019 Discrimination of dynamically and post-dynamically recrystallized grains based on EBSD data. Application to Inconel 718. *J. Microsc*. **273** 135-147